Send Orders for Reprints to reprints@benthamscience.net

 Current Inorganic Chemistry, **2013,** *3,* **220-234**

Exploring Bonding in Heavy Atom Chemistry with Dirac-Exact Methods

Wenli Zou, Michael Filatov and Dieter Cremer*

CATCO, Department of Chemistry, Southern Methodist University, 3215 Daniel Ave, Dallas, Texas 75275-0314, USA

Abstract: The normalized elimination of the small component (NESC) method is a first principles 2-component relativistic approach that leads to the Dirac-exact description of one-electron systems. It is a powerful method to routinely investigate chemical and physical properties of molecules containing relativistic atoms. The vibrational modes of mercury halides are investigated to derive via the corresponding local HgX (X = H, F, Cl, Br, I, At) stretching modes an appropriate measure for the HgX bond strength. It is shown that HgF bonding in HgF_4 is stronger than that in HgF_2, which is a result of enhanced charge transfer from Hg to the four F atoms and the formation of electron deficient 2e-4c bonds with strong ionic character. A generally applicable bonding model for HgX molecules is outlined.

Keywords: Dirac-exact relativistic methods, local vibrational modes, mercury bonding, Normalized Elimination of the Small Component (NESC), spin-orbit coupling,.

1. INTRODUCTION

The influence of relativistic effects [1] on the electronic structure and the chemical properties of molecules containing heavy elements (in short *relativistic* elements) is well-documented in the literature [2-13]. Relativistic effects change the nature of chemical bonding and by this the stability and reactivity of molecules. Spectroscopic properties such as vibrational frequencies, infrared intensities, magnetic shielding, NMR spin-spin coupling constants, etc. adopt characteristically different values under the impact of relativity.

The relativistic counterpart of the Schrödinger equation is the Dirac equation [14, 15], which provides the basis for an exact description of a single electron in an external field. The step from a single electron to a multiple electron problem requires relativistic calculations both for the one-electron and the two-electron part of the Hamiltonian. The quantum mechanical methodology to reliably calculate molecular properties of molecules containing relativistic atoms developed much slower than its non-relativistic counterpart. In the last 15 years, the Dirac-exact relativistic methods have been developed, which lead to accurate 4-component results with a 2-component or even 1-component approach.

The first Dirac-exact relativistic 2-component method was developed by Dyall [16] in form of the normalized elimination of the small component (NESC) approach. Dyall developed the NESC method at a time when most quantum chemists followed an operator-driven strategy to convert Dirac's four-component description by a series of transformations into a two-component one. Contrary to these attempts, he attacked the problem by starting from a matrix formulation of the Dirac equation and then carried out all the pertinent transformations by adhering to the matrix formulation [17-19]. Dyall's NESC formalism is computationally simple and enables one to obtain the exact electronic (positive-energy) solutions of the Dirac equation as was demonstrated by Zou and co-workers [20]. The success of a matrix-driven methodology has led to a subsequent development of alternative Dirac-exact methods based on matrix formulations [21-24]. These have been proved to be equivalent to NESC [25]. It is also noteworthy that approximate relativistic methods based on the so-called regular approximation [26-30] can be easily derived from NESC, which leads to a simple matrix formulation of these methods [31, 32].

A relativistic method as any quantum chemical method has to fulfill a number of criteria to be accepted by the community of computational chemists. It must be accurate and at the same time cost-efficient to be applicable to non-trivial chemical problems. Furthermore, it is important that molecular properties can be routinely calculated with the method in question. The largest group of molecular properties are the response properties as, for example, the molecular forces (needed to determine the equilibrium geometry of a molecule), electric or magnetic moments, polarizabilities, spectroscopic quantities, etc. Their calculation requires the availability of analytic energy derivatives and therefore much of the recent work with the NESC method has focused on the development of a NESC derivative formalism [33-39].

Due to the availability of NESC analytic derivatives, the calculation of first order and second order response properties with NESC has become routine. In this article, we will emphasize the need of accurately calculating vibrational properties of molecules containing relativistic atoms. For this purpose, we will briefly outline some basics of the NESC method and the NESC energy derivatives formalism. Then, we will focus on the description of mercury bonding and on how its peculiarities can be assessed using vibrational modes.

*Address correspondence to this author at the CATCO, Department of Chemistry, Southern Methodist University, 3215 Daniel Ave, Dallas, Texas 75275-0314, USA; E-mail: dieter.cremer@gmail.com

1877-945X/13 $58.00+.00 © 2013 Bentham Science Publishers

2. BRIEF OVERVIEW OVER THE NESC METHOD

The NESC equations were derived from the modified Dirac equation in matrix form:

$$\begin{pmatrix} \mathbf{V} & \mathbf{T} \\ \mathbf{T} & \mathbf{W}-\mathbf{T} \end{pmatrix}\begin{pmatrix} \mathbf{A}_- & \mathbf{A}_+ \\ \mathbf{B}_- & \mathbf{B}_+ \end{pmatrix}=\begin{pmatrix} \mathbf{S} & \mathbf{0} \\ \mathbf{0} & (2mc^2)^{-1}\mathbf{T} \end{pmatrix}\begin{pmatrix} \mathbf{A}_- & \mathbf{A}_+ \\ \mathbf{B}_- & \mathbf{B}_+ \end{pmatrix}\begin{pmatrix} \varepsilon^- & \mathbf{0} \\ \mathbf{0} & \varepsilon^+ \end{pmatrix} \quad (1)$$

where **A** and **B** are the matrices collecting the expansion coefficients of the large and pseudo-large components of the relativistic wavefunction in terms of the basis functions χ_μ^L (or χ_μ for brevity) and the diagonal matrix ε contains the energy eigenvalues. The superscripts or subscripts + and - denote the positive (electronic) and negative (positronic) eigenvalue and eigenvector solutions of the equation. Symbols **S**, **T**, and **V** represent the non-relativistic overlap, kinetic energy, and potential energy matrices, respectively, and **W** is the matrix of the operator $(1/4m^2c^2)(\boldsymbol{\sigma}\cdot\mathbf{p})V(\mathbf{r})(\boldsymbol{\sigma}\cdot\mathbf{p})$, which can be separated according to Eq. (2):

$$\mathbf{W}=\mathbf{W}^{sf}+i\boldsymbol{\sigma}\cdot\mathbf{W}^{SO} \quad (2)$$

By neglecting the spin-dependent part $\mathbf{W}^{SO}$ the spin-scalar approximation is obtained, which is used in the following.

Dyall was able to eliminate the small (pseudo-large) component from the modified Dirac equation and to simultaneously project eigenvalues onto the positive energy (electronic) states [16]. Focusing on the electronic states only and dropping the + superscript, the working equations of the NESC method are given by Eq. (3):

$$\tilde{\mathbf{L}}\mathbf{A}=\tilde{\mathbf{S}}\mathbf{A}\boldsymbol{\varepsilon} \quad (3a)$$

$$\tilde{\mathbf{L}}=\mathbf{U}^\dagger\mathbf{T}+\mathbf{T}\mathbf{U}-\mathbf{U}^\dagger\left(\mathbf{T}-\mathbf{W}\right)\mathbf{U}+\mathbf{V} \quad (3b)$$

$$\tilde{\mathbf{S}}=\mathbf{S}+\frac{1}{2mc^2}\mathbf{U}^\dagger\mathbf{T}\mathbf{U} \quad (3c)$$

where the NESC Hamiltonian $\tilde{\mathbf{L}}$ and the NESC large component metric $\tilde{\mathbf{S}}$ are introduced. Matrix **U** is associated with the elimination of the small component and can be calculated either iteratively [20] or in a one-step approach [16, 20] that uses the solutions of the modified Dirac equation (1):

$$\mathbf{U}=\mathbf{B}_+\mathbf{A}_+^\dagger\left(\mathbf{A}_+\mathbf{A}_+^\dagger\right)^{-1}=\mathbf{B}_+\mathbf{A}_+^\dagger\tilde{\mathbf{S}} \quad (4)$$

The one-electron approximation defined in this way is a sufficiently accurate approximation to the many-electron relativistic self-consistent field (SCF) approach. Using Hartree-Fock theory, the atomic or molecular Fock operator adopts the form of Eq. (5):

$$\mathbf{F}^{NESC}=\mathbf{G}^\dagger\tilde{\mathbf{L}}\mathbf{G}+\left(\mathbf{J}-\mathbf{K}\right)=\mathbf{H}_{1e}+\left(\mathbf{J}-\mathbf{K}\right) \quad (5)$$

where **J** and **K** correspond to the Coulomb and exchange contributions to the two-electron part of the non-relativistic Fock matrix. The renormalization matrix **G** enters the equation for the Fock matrix because the one-electron NESC Hamiltonian has to be transformed from the relativistic normalization of the electronic wavefunction to the non-relativistic normalization [40]:

$$\mathbf{G}=\mathbf{S}^{-1/2}\left(\mathbf{S}^{1/2}\tilde{\mathbf{S}}^{-1}\mathbf{S}^{1/2}\right)^{1/2}\mathbf{S}^{1/2} \quad (6)$$

The total energy of a many-electron system in the relativistic 1*e* -approximation is given by Eq. (7):

$$E^{NESC}=\mathrm{tr}\mathbf{P}\mathbf{H}_{1e}+\frac{1}{2}\mathrm{tr}\mathbf{P}\left(\mathbf{J}-\mathbf{K}\right) \quad (7)$$

where $\mathbf{P}=\mathbf{C}\mathbf{n}\mathbf{C}^\dagger$ is the density matrix constructed using the eigenvectors **C** of the Fock operator (5) and the diagonal matrix of the orbital occupation numbers **n**. Further details on the implementation of the NESC method can be found in the original publication [20].

When differentiating the NESC total energy (7) with respect to an arbitrary external perturbation parameter λ, one obtains Eq. (8):

$$\frac{\partial E}{\partial\lambda}=\mathrm{tr}\mathbf{P}\left(\frac{\partial\mathbf{H}_{1e}}{\partial\lambda}\right)+\frac{1}{2}\mathrm{tr}\mathbf{P}\frac{\partial'}{\partial\lambda}(\mathbf{J}-\mathbf{K})+\mathrm{tr}\boldsymbol{\Omega}\left(\frac{\partial\mathbf{S}}{\partial\lambda}\right) \quad (8)$$

where $\boldsymbol{\Omega}=-\mathbf{C}\mathbf{n}\boldsymbol{\varepsilon}\mathbf{C}^\dagger$ is the energy-weighted density matrix (Lagrangian) and the prime at $\frac{\partial'}{\partial\lambda}$ implies that only the two-electron integrals have to be differentiated [33].

The first term in Eq. (8) can be explicitly written as:

$$\mathrm{tr}\mathbf{P}\left(\frac{\partial\mathbf{H}_{1e}}{\partial\lambda}\right)=\mathrm{tr}\mathbf{P}\mathbf{G}^\dagger\frac{\partial\tilde{\mathbf{L}}}{\partial\lambda}\mathbf{G}+\mathrm{tr}\mathbf{P}\frac{\partial\mathbf{G}^\dagger}{\partial\lambda}\tilde{\mathbf{L}}\mathbf{G}+\mathrm{tr}\mathbf{P}\mathbf{G}^\dagger\tilde{\mathbf{L}}\frac{\partial\mathbf{G}}{\partial\lambda} \quad (9a)$$

$$=\mathrm{tr}\tilde{\mathbf{P}}\frac{\partial\tilde{\mathbf{L}}}{\partial\lambda}+\mathrm{tr}\mathbf{D}\frac{\partial\mathbf{G}^\dagger}{\partial\lambda}+\mathrm{tr}\mathbf{D}^\dagger\frac{\partial\mathbf{G}}{\partial\lambda} \quad (9b)$$

where new matrices $\tilde{\mathbf{P}}=\mathbf{G}\mathbf{P}\mathbf{G}^\dagger$ and $\mathbf{D}=\tilde{\mathbf{L}}\mathbf{G}\mathbf{P}$ are introduced. Differentiating Eq. (3b) with respect to λ and inserting the derivative into the first term of Eq. (9b) yields:

$$\mathrm{tr}\tilde{\mathbf{P}}\frac{\partial\tilde{\mathbf{L}}}{\partial\lambda}=\mathrm{tr}(\mathbf{U}\tilde{\mathbf{P}}+\tilde{\mathbf{P}}\mathbf{U}^\dagger-\mathbf{U}\tilde{\mathbf{P}}\mathbf{U}^\dagger)\frac{\partial\mathbf{T}}{\partial\lambda}+\mathrm{tr}(\mathbf{U}\tilde{\mathbf{P}}\mathbf{U}^\dagger)\frac{\partial\mathbf{W}}{\partial\lambda}+\mathrm{tr}\tilde{\mathbf{P}}\frac{\partial\mathbf{V}}{\partial\lambda} \quad (10a)$$

$$+\mathrm{tr}(\mathbf{T}-(\mathbf{T}-\mathbf{W})\mathbf{U})\tilde{\mathbf{P}}\frac{\partial\mathbf{U}^\dagger}{\partial\lambda}+\mathrm{tr}\tilde{\mathbf{P}}(\mathbf{T}-\mathbf{U}^\dagger(\mathbf{T}-\mathbf{W}))\frac{\partial\mathbf{U}}{\partial\lambda} \quad (10b)$$

These equations have been solved by Zou, Filatov, and Cremer [33] where both high accuracy and routine calculations of the derivatives $\partial\mathbf{G}/\partial\lambda$ and $\partial\mathbf{U}/\partial\lambda$, respectively, have been worked out [33]. The first derivative formalism of the NESC method was the basis for the development of specific first order response properties such as the hyperfine parameters [34-36, 39].

For the second order response properties such as the vibrational frequencies, analytical second derivatives of the NESC energy are required, which were derived by Zou, Filatov, and Cremer [37]. Starting from Eq. (8), the second derivatives can be calculated as:

$$\begin{aligned}\frac{\partial^2 E}{\partial\mu\partial\lambda}=&\mathrm{tr}\Omega\frac{\partial^2\mathbf{S}}{\partial\mu\partial\lambda}+\mathrm{tr}\mathbf{P}\frac{\partial^2\mathbf{H}_{1\text{-}e}}{\partial\mu\partial\lambda}+\frac{1}{2}\mathrm{tr}\mathbf{P}\frac{\partial^{2\prime}}{\partial\mu\partial\lambda}(\mathbf{J}-\mathbf{K})\\&+\mathrm{tr}\frac{\partial\Omega}{\partial\mu}\frac{\partial\mathbf{S}}{\partial\lambda}+\mathrm{tr}\frac{\partial\mathbf{P}}{\partial\mu}\frac{\partial\mathbf{H}_{1\text{-}e}}{\partial\lambda}+\frac{1}{2}\mathrm{tr}\frac{\partial\mathbf{P}}{\partial\mu}\frac{\partial'}{\partial\lambda}(\mathbf{J}-\mathbf{K})\end{aligned} \quad (11)$$

The first and the third term in Eq. (11) are determined utilizing the standard non-relativistic methodology. The derivatives $\partial \mathbf{P} / \partial \mu$ and $\partial \mathbf{\Omega} / \partial \mu$ are obtained from the coupled perturbed (CP) equations [41, 42], which employ the derivatives $\partial \mathbf{H}_{1-e} / \partial \mu$.

For the second to last term of Eq. (11), the derivative matrix $\partial \mathbf{H}_{1-e} / \partial \lambda$ can be obtained with the help of Eq. (9). By differentiating Eq. (9) another time, one obtains the second derivative of the renormalized NESC Hamiltonian and thereby also the second term of Eq. (11):

$$\frac{\partial^2 \mathbf{H}_{1-e}}{\partial\mu\partial\lambda} = \frac{\partial^2 \mathbf{G}^\dagger}{\partial\mu\partial\lambda}\tilde{\mathbf{L}}\mathbf{G} + \mathbf{G}^\dagger\tilde{\mathbf{L}}\frac{\partial^2 \mathbf{G}}{\partial\mu\partial\lambda} + \mathbf{G}^\dagger\frac{\partial^2 \tilde{\mathbf{L}}}{\partial\mu\partial\lambda}\mathbf{G} + \frac{\partial \mathbf{G}^\dagger}{\partial\mu}\tilde{\mathbf{L}}\frac{\partial \mathbf{G}}{\partial\lambda} + \frac{\partial \mathbf{G}^\dagger}{\partial\lambda}\tilde{\mathbf{L}}\frac{\partial \mathbf{G}}{\partial\mu} + \frac{\partial \mathbf{G}^\dagger}{\partial\mu}\frac{\partial \tilde{\mathbf{L}}}{\partial\lambda}\mathbf{G} + \frac{\partial \mathbf{G}^\dagger}{\partial\lambda}\frac{\partial \tilde{\mathbf{L}}}{\partial\mu}\mathbf{G} + \mathbf{G}^\dagger\frac{\partial \tilde{\mathbf{L}}}{\partial\lambda}\frac{\partial \mathbf{G}}{\partial\mu} + \mathbf{G}^\dagger\frac{\partial \tilde{\mathbf{L}}}{\partial\mu}\frac{\partial \mathbf{G}}{\partial\lambda} \quad (12)$$

$$\mathrm{tr}\mathbf{P}\frac{\partial^2 \mathbf{H}_{1-e}}{\partial\mu\partial\lambda} = \mathrm{tr}\mathbf{P}\frac{\partial^2 \tilde{\mathbf{L}}}{\partial\mu\partial\lambda} + \mathrm{tr}\left(\mathbf{D}\frac{\partial^2 \mathbf{G}^\dagger}{\partial\mu\partial\lambda} + \mathbf{D}^\dagger\frac{\partial^2 \mathbf{G}}{\partial\mu\partial\lambda}\right) + \mathrm{tr}\mathbf{P}\left[\left(\frac{\partial \mathbf{G}^\dagger}{\partial\mu}\frac{\partial \tilde{\mathbf{L}}}{\partial\lambda} + \frac{\partial \mathbf{G}^\dagger}{\partial\lambda}\frac{\partial \tilde{\mathbf{L}}}{\partial\mu}\right)\mathbf{G} + \mathbf{G}^\dagger\left(\frac{\partial \tilde{\mathbf{L}}}{\partial\lambda}\frac{\partial \mathbf{G}}{\partial\mu} + \frac{\partial \tilde{\mathbf{L}}}{\partial\mu}\frac{\partial \mathbf{G}}{\partial\lambda}\right)\right] + \mathrm{tr}\mathbf{P}\left(\frac{\partial \mathbf{G}^\dagger}{\partial\mu}\tilde{\mathbf{L}}\frac{\partial \mathbf{G}}{\partial\lambda} + \frac{\partial \mathbf{G}^\dagger}{\partial\lambda}\tilde{\mathbf{L}}\frac{\partial \mathbf{G}}{\partial\mu}\right) \quad (13)$$

In Eq. (13) the first and second derivatives of matrix **G** can be calculated as described by Zou and co-workers [37]. The derivatives of the elements of the renormalization matrix **G** with respect to the nuclear displacements are small due to the fact that the renormalization matrix **G** is sufficiently close to a unit matrix for all the basis functions except for the tightest ones. For the latter basis functions however, the dependence of the matrix elements of **G** on the molecular geometry is the weakest. Consequently, the contribution of the last term of Eq. (13) is on the order of 10^{-7} a.u. or less. Hence, this term can be neglected for the calculation of vibrational frequencies.

3. THE NEED FOR CALCULATING VIBRATIONAL FREQUENCIES

The routine investigation of relativistic molecules implies the calculation of second order response properties such as vibrational frequencies [41, 37, 38]. The latter are of enormous importance for relating calculated molecular energies to measured enthalpies. Most experiments are carried out at room temperature and molecular stabilities are measured in terms of enthalpy differences such a combustion or hydrogenation enthalpies, which are then converted into heats-of-formation utilizing the known heats-of-formations of the elements and some small molecules [43, 44]. Quantum chemical calculations can only provide energy differences at 0 K, which can significantly differ from enthalpy differences at room temperature due to the influence of zeropoint energies as well as other vibrational and thermochemical corrections. For the purpose of converting energy differences into enthalpy differences, the vibrational frequencies of a molecule must be known.

Many relativistic atoms or molecules are present in aqueous solution in form of hydrated cations. The energetics of their reactions is measured in terms of free energy differences rather than enthalpy differences because changes in the ligand shell of a cation can lead to significant entropy changes, which can also have an influence on the reactivity of a given species. The magnitudes of entropies depend on translational, rotational, and vibrational contributions where the calculation of the latter again requires the knowledge of the vibrational frequencies. Hence, a careful study of the reactions of relativistic species in aqueous solution requires the calculation of free energy differences $\Delta G^o_{298} = \Delta H^o_{298} - T\Delta S^o_{298}$, which is only possible if vibrational frequencies are available in this medium.

There is also the need for vibrational frequencies in connection with the investigation of chemical bonding. The stretching frequency and the stretching force constant of a given bond are closely connected to its bond strength. Therefore, one has made numerous attempts to relate stretching frequencies or force constants to other bond properties. Alternatively, one can directly use these properties as suitable bond strength descriptors.

3.1. Stretching Force Constants as Bond Strength Descriptors

The basis for our understanding of the chemical bond was cemented by the pioneering work of Pauling [45], Slater [46] and Mulliken [47] who showed that the strength of a bond depends on the degree of overlap between the interacting atomic orbitals and the bond polarity reflected by the difference in the energies of the atomic orbitals involved in bonding. Accordingly, the bond strength is determined by covalent (overlap) and ionic effects (bond polarity). There are many attempts to computationally assess the covalent and/or ionic character of a bond and to derive from these a suitable bond strength descriptor. However, these attempts are of little use if they cannot be related to a measured bond property, which reflects the strength of a bond. Commonly, this is done by referring to measured bond dissociation enthalpies (BDH) [44] or calculated bond dissociation energies (BDEs), which differ by vibrational and temperature corrections.

Both BDE and BDH values partly depend on the strength of the bond to be broken and partly on the stabilization of the fragments to be formed. The latter can lower their energy by geometry relaxation and orbital rehybridization. This leads to changes in the electron density distribution and thereby to an energy lowering. In recent work, we have shown that these relaxation effects vary significantly from case to case [48, 49] and accordingly the BDE and BDH values are poor bond strength descriptors.

Similar problems arise if one tries to use the bond length as a bond strength descriptor. Although most chemists expect that bond shortening (lengthening) indicates bond strengthening (weakening), there are many examples that do not follow this expectation [50]. This can be explained when assuming that the bond length is approximated by the sum of the covalent radii of the atoms being bonded. The covalent radius depends on the number of core shells and the charge of an atom. Clearly, it is smaller for a positively and larger for a negatively charged atom, i.e. it depends on the bonding partners of a given atom. For example, if several fluorine atoms are bonded to a N or O atom, the positive charge of the central atom (N, O) increases and its covalent radius and by this the NF (OF) bond lengths decrease. At the same time, an increase of lone-lone pair repulsion leads to a weakening

of the NF (OF) bond with the result that the weaker bond is the shorter bond.

A similar situation can occur in the case of bonds involving relativistic atoms. For example, mercury undergoes bonding by donating 6s-electrons to its bonding partner. The relativistic contraction of the 6s-orbitals decreases its covalent radius and thereby the bond length. This contraction implies also that the charge transfer to the bonding partner is reduced so that a weaker bond results. Again, the shorter bond indicates bond weakening rather than bond strengthening in contrast to normal predictions. In conclusion, bond length and BDE value can be at best qualitative bond strength descriptors provided their usefulness is confirmed in each case by applying other, more reliable descriptors.

The BDE can be considered as a dynamic bond strength descriptor because it is associated with the dynamic process of bond dissociation. In view of the fact that bond dissociation leads to a drastic change in the electronic structure of the targeted molecule, its BDE value cannot be a bond strength descriptor in the quantitative sense. Following this line of thought, a quantitative descriptor should result when the bond strength is probed with an infinitesimally small change of the bond thus excluding any electronic structure changes in the molecule. Such a situation is realized in a bond stretching vibration.

A bond stretching vibration probes the strength of the bond by a small displacement of the nuclei from their equilibrium positions, which is accompanied by a small but finite electronic structure change [48]. However, the force constant of the stretching vibration corresponds to an infinitesimally small displacement, which does not imply any electronic structure changes of the molecule, but nevertheless reflects the strength of the bond. Hence, reliable bond strength information can be gained from of measured or calculated vibrational spectra provided suitable stretching force constants can be obtained from the spectral analysis.

The description of the chemical bond with the help of the stretching force constants and frequencies of the vibrational spectra dates back to the 20ies and 30ies of the last century when Badger [51] found a power relationship between the force constant and the bond length for diatomic molecules. The extension of these relationships to polyatomic molecules turned out to be difficult because the stretching vibrations are never localized in a bond, which is the result of a coupling between the vibrational modes. Accordingly, the spectroscopically derived stretching force constants are not unique, reflect mode-mode coupling, and depend on the internal coordinates used for the description of a molecule [50].

During the last 60 years, many attempts have been made to determine stretching force constants, which can be used as bond strength descriptors. Many of these attempts were empirically based and focused on a special bond type found in a relatively small numbers of molecules [50]. On the theoretical side, one tried to derive suitable procedures for determining *local vibrational modes*, which are localized in a molecular unit, e.g. a diatomic unit associated with a bond. At an early stage, one realized that local parameters can be obtained by inverting the basic equations of vibrational spectroscopy [52]. Decius [7] and others [54, 55] used the inverse force constant matrix and introduced the compliance constants Γ_n (associated with internal coordinate q_n) as potential bond strength descriptors. Ample work has been carried out with the compliance constants to describe the properties of chemical bonds [56-58] although their physical meaning and relationship to the normal vibrational modes remained unclear.

McKean [59-61] solved the problem of obtaining local stretching force constants in an approximate way by measuring *isolated* XH stretching frequencies for a suitable isotopomer of a given target molecule. The 2:1 mass ratio of deuterium to hydrogen leads to partial mass-decoupling of the vibrational modes and XH stretching frequencies and force constants of approximate local vibrational modes can be measured. Henry [62] pioneered the technique of obtaining local mode information from overtone spectra. Apart from these examples, there were numerous attempts to set up relationships between stretching force constants or frequencies and bond strength descriptors such as BDE values, bond orders, bond lengths, etc., which are discussed in a 2010 review article that underlines the necessity of obtaining local mode information from normal vibrational modes [50].

Analyzing McKean's work on isolated CH stretching frequencies, Konkoli and Cremer realized that local vibrational modes can be easily obtained by solving the Euler-Lagrange equations in a mass-decoupled form [63-67]. Recently, it was proved that the Konkoli-Cremer modes are unique and the only local modes that directly relate to the normal vibrational modes when solving the basic equations of vibrational spectroscopy [85, 86]. Furthermore, the stretching force constants obtained with the local vibrational modes fulfill all criteria for deriving reliable bond strength descriptors. A number of investigations document the usefulness of the local vibrational modes [49, 50, 67, 69-73]. In the following, the procedure for determining local vibrational modes and their properties is shortly outlined:

The basic equation of vibrational spectroscopy is given by [74]:

$$\mathbf{F}^q\mathbf{D} = \mathbf{G}^{-1}\mathbf{D}\boldsymbol{\Lambda} \qquad (14)$$

where $\mathbf{F}^q$ is the force constant matrix in internal coordinates, $\mathbf{G}$ is Wilson's kinetic energy matrix, $\mathbf{D}$ collects the normal mode vectors in internal coordinates, and $\boldsymbol{\Lambda}$ is a diagonal matrix with $3N - L = N_{vib}$ vibrational eigenvalues $\lambda_\mu = 4\pi^2c^2\omega_\mu^2$ (ω_μ : frequency of normal mode μ; c : speed of light; N : number of atoms in the molecule; L : number of translational and rotational degrees of freedom). Diagonalization of the force constant matrix yields the matrix $\mathbf{K} = \mathbf{D}^\dagger\mathbf{F}^q\mathbf{D}$ that contains the force constants k_μ associated with frequency ω_μ of a given mode μ on its diagonal.

Once the diagonal force constant matrix $\mathbf{K}$ and the mode eigenvectors collected in matrix $\mathbf{D}$ are obtained it is straightforward to determine the local mode vectors $\mathbf{a}_n$ of a molecule by [63]:

$$\mathbf{a}_n = \frac{\mathbf{K}^{-1}\mathbf{d}_n^{\dagger}}{\mathbf{d}_n\mathbf{K}^{-1}\mathbf{d}_n^{\dagger}} \quad (15)$$

where $\mathbf{d}_n$ is a row vector of matrix **D** associated with the internal coordinate $\mathbf{q}_n$. The local mode force constant k_n^a is given by Eq. (16):

$$k_n^a = \mathbf{a}_n^{\dagger}\mathbf{K}\mathbf{a}_n \quad (16)$$

and the local mode frequency ω_n^a can be obtained from:

$$(\omega_n^a)^2 = \frac{G_{nn}k_n^a}{4\pi^2c^2} \quad (17)$$

where the **G**-matrix element G_{nn} corresponds to the reciprocal of the local mode mass [63]. In these equations, the superscript a refers to the adiabatic nature of the local vibrational modes: With a finite displacement of the nuclei involved in a local mode, the positions of the remaining atoms of the molecule are adiabatically relaxed, which leads to a decoupling from other modes in the molecule.

A local mode depends only on the internal coordinate, which drives the movement of the nuclei (*leading parameter principle* [63]). Apart from this coordinate, it is independent of all other internal coordinates used to describe the geometry of a molecule. Accordingly, it is also independent of whether redundant or non-redundant coordinate sets are used. Another advantage of the local vibrational modes is that they confer for the first time physical meaning to the compliance constants Γ_n of Decius [53]. Zou and co-workers [68, 69] proved that $1/\Gamma_n = k_n^a$, i.e. the reciprocal of the compliance constant is equal to the local mode force constants and thereby the compliance constants can be associated with a physically well-defined mode and its properties. As was shown by Cremer and co-workers, local mode frequencies and force constants can be determined from a complete set of $3N - L$ measured normal frequencies utilizing perturbation theory [67]. In this way, one can distinguish between calculated harmonic local mode frequencies (force constants) and experimentally-based local mode frequencies (force constants), which differ by anharmonicity effects [72, 73]. Konkoli and Cremer showed that each normal vibrational mode can be characterized in terms of local vibrational modes, where their Characterization of Normal Mode (CNM) method is superior to the potential energy distribution analysis [64, 50]. Most important is that local mode frequencies can be directly related to normal mode frequencies with the help of an adiabatic connection scheme (ACS), which reveals the kinematic coupling mechanism between the local modes such that the results of the CNM analysis can be physically explained [68, 69].

The local stretching force constants represent reliable bond strength descriptors [50, 67-69, 72, 73, 75], which for the purpose of facilitating the analysis, are converted into bond orders if bonds of the same type are compared or, alternatively, relative bond strength orders (RBSO) if different types of bonds are compared. To determine the RBSO value of a bond, at least two suitable reference bonds have to be chosen, which, for example, represent a typical single or double bond according to common chemical understanding. If two suitable reference bonds cannot be defined, one has to make use of the Badger rule [51] or its extension given by Kraka and co-workers [49, 50]. According to Badger, stretching force constants k and bond lengths r of diatomic molecules follow one common power relationship, provided only atoms from the same period of the periodic table are involved in bonding. Kraka and co-workers extended the Badger-rule to polyatomic molecules by using local stretching force constants [50, 75]. Their extension of the Badger rule says: *Different bonds can be described by one common power relationship relating local mode stretching force constants to RBSO values as suitable bond strength descriptors.* Since Badger's rule focuses on bond lengths and their dependence on the covalent radii of the atoms, its application is limited. The extended Badger rule considers the relationship between stretching force constants, which is not limited to bonding between atoms of the same period(s). Accordingly, there is chance of using one and the same power relationship between stretching force constants k^a and RBSO values n for HgX bonds with X representing an arbitrary bonding partner.

The approach of describing the bond strength via the local stretching force constant is based on features of the adiabatic Born-Oppenheimer potential energy surface (PES) as it is described by measured or calculated spectroscopic constants. Hence, in all those cases where the Born-Oppenheimer approximation is no longer valid as, e.g., in the case of nonadiabatic effects, the local mode description, which is closely connected to the concept of an adiabatic PES, can no longer be applied. However, as long as molecules in their equilibrium geometry are investigated this problem does not arise.

Apart from this, one has to consider also other potential shortcomings of the local mode description of the bond strength: i) The Wilson equation (14) does not provide a quantum mechanical description of vibrating molecules. ii) Vibrational frequencies are normally calculated using the harmonic approximation. If the anharmonicity effects are large, harmonic local stretching force constants can significantly differ from their anharmonically corrected counterparts. In these cases, the focus of a bond strength analysis should be more on general trends observed in related systems rather than individual RBSO values. Alternatively, one can calculate anharmonicity corrections and derive local mode frequencies based on the corrected frequencies [72, 73]. iii) The accuracy of the computed frequencies depends on the method and basis set used. Their influences has to be analyzed for each case, which however is a standard approach for all calculated molecular properties.

In view of the importance of local stretching vibrations when investigating bonding between relativistic atoms, there is a need to determine normal vibrationals modes with Dirac-exact methods, which in turn requires the availability of suitable formalism to calculate second order response properties from analytical second energy derivatives.

3.2. From Mono- and Bivalent to Tetravalent Mercury

Mercury has a $[Xe]4f^{14}5d^{10}6s^{2}$ electron configuration, which leads to some similarity with Be and other elements with an ns^2 electron configuration. Bonding of Hg is strongly affected by relativistic effects as is reflected by its first three ionization potentials (IP) (see Table **1**). For group 15 to group 18 elements of period 4, 5, and 6, the first IP (IP1) decreases with increasing atomic number. However, for Hg the trend is different: The first IP (IP1) decreases from Zn to Cd, which is in line with the increased screening of the nucleus by the 4d-shell. Then, for Hg the value of IP1 increases again as a direct consequence of the mass-velocity effect that leads to a contraction of the 6s orbital, a lowering of the 6s-orbital energy and a subsequent increase of IP1. Actually, this effect should be strongest for the 1s-electrons of Hg whereas the valence s-orbitals should not experience a relativistic contraction. However, one has to consider the orthogonality of the orbitals and the fact that any relativistic distortion of the 1s orbital leads to similar distortions of the outer s-orbitals, i.e. the 1s contraction occurs for the 2s, 3s, 4s, 5s, and 6s orbitals as well.

Similar observations can be made for the ionization of the second 6s electron (see IP2 in Table **1**), the first three IPs of Tl associated with the ionization of its $6s^{2}6p^{1}$ electrons, and the IP1 of Au (Table **1**). In this connection, it has to be mentioned that spin-orbit coupling leads to a contraction of the $6p_{1/2}$ spinor in line with that of $6s_{1/2}$ (the corresponding spinors are both spherically symmetric) whereas the $6p_{3/2}$ spinor occupied for Bi, Po, etc. expands and has a higher energy thus leading to a lowering of IP1.

The mass-velocity effect in the case of the 6s-electrons would be even stronger, if the Darwin-effect would not partly compensate the former. The Darwin effect is responsible for an oscillatory motion of the electron (*Zitterbewegung*) that is especially important close to the nucleus. Consequently, the 6s orbital expands and its energy is somewhat raised when just the Darwin-effect is considered.

The IP3 of Hg is associated with the ionization of a 5d electron. Since the d-orbitals expand due to a more effective screening of the Hg nucleus by the s-electrons, their orbital (spinor) energies are higher and IP3 becomes lower (see Table **1**). A similar effect is observed for IP2 and IP3 of Au, which facilitates the oxidation to Au(II) and Au(III) compounds. For Hg, the expansion of the 5d-orbitals is the actual reason for the formation of $Hg(IV)X_4$ molecules, which cannot be realized for its lower homologues Cd and Zn because a similar d-expansion effect accompanied by a lowering of the d-ionization potentials is missing there.

According to the IUPAC nomenclature, mercury is not a transition metal because neither the atom itself nor its cations in the most commonly occurring oxidation states (I and II) possess an incomplete d-subshell [77]. Although the Hg(IV)-compounds would fall under the IUPAC definition of a transition metal (as the Hg(IV) cation possesses partially filled d-subshell [78]), one can still argue that Hg(IV) compounds are not generated under ambient chemical conditions [78] and, therefore, Hg still fails to be a transition metal [77]. In the present work, we leave out the discussion whether mercury is a transition metal or not, as this is an unresolved issue that bears little scientific benefit, and focus on the impact that relativity has on Hg-bonding in general and especially on Hg(IV)-bonding.

In Fig. (**1**), 25 BDE values (in blue) and their scalar relativistic correction (in red) of molecules HgX are shown according to NESC/CCSD(T) calculations of Cremer and co-workers [79] carried out with a contracted [15s13p8d5f] basis set for Hg where the contraction was done to minimize the basis set superposition error (BSSE). Substituents X contain a main group element from the 2nd, 3rd, 4th, and 5th period. As revealed by the BDE values in Fig. (**1**), the non-relativistic BDE values are overestimated by 1- 32 kcal/mol where the scalar relativistic corrections are largest for strongly electronegative groups X and smallest for electropositive X such as the alkali metals (1.5 kcal/mol for X = Rb).

The trend in the scalar relativistic corrections becomes understandable when the molecular orbitals (MOs) of HgX are analyzed. In Fig. (**2**), the nine highest occupied MO levels of $HgF(^{2}\Sigma^{+})$ together with some MOs drawings are

Table 1. Comparison of ionization potentials for group 11, 12, and 13 elements. [a]

Group	Element	IP1	IP2	IP3
11	Cu	7.726	20.292	36.841
	Ag	7.576	21.484	(34.83)
	Au	9.225	20.203	(30.0)
12	Zn	9.394	17.964	39.722
	Cd	8.994	16.908	37.468
	Hg	10.437	18.757	34.467
13	Ga	5.999	20.515	30.726
	In	5.786	18.870	28.044
	Tl	6.108	20.428	29.852

[a]Measured first, second, and third ionization potential (IP1, IP2, IP3) in eV taken from the NIST tables [76]. Values in parentheses correspond to calculated data.

H	21.2 -11.1										
Li	5.3 -2.4	**CH_3**	10.4 -7.4	**NH_2**	17.1 -12.9	**OH**	34.1 -21.8	**O**	26.8 -23.0	**F**	62.6 -31.7
Na	3.6 -1.3	**SiH_3**	13.1 -6.8	**PH_2**	11.5 -7.9	**SH**	25.9 -16.2	**S**	23.0 -17.3	**Cl**	46.8 -25.4
K	2.5 -1.8	**GeH_3**	13.4 -8.0	**AsH_2**	10.3 -5.8	**SeH**	22.7 -15.1	**Se**	19.7 -16.0	**Br**	39.8 -25.3
Rb	2.2 -1.5	**SnH_3**	11.5 -8.5	**SbH_2**	8.0 -4.0	**TeH**	18.2 -11.4	**Te**	16.2 -13.6	**I**	31.3 -20.4

nonrelativistic Hg-X energies relativistic correction

Fig. (1). Non-relativistic BDE values (blue) calculated at the CCSD(T) level of theory and their relativistic NESC corrections (red) for 25 HgX molecules [79].

shown. The 5d(Hg) orbitals split up into two non-bonding MOs ($5d_{x^2-y^2}$ and $5d_{xy}$), a $\sigma(5d_{z^2})$ MO, and two π-type MOs ($5d_{xz}$ and $5d_{yz}$) where the latter combine with the F orbitals of σ and π symmetry. The highest doubly occupied HgF MOs are of the π-, σ-, and π^*-type. The HOMO corresponds to a singly occupied σ^* MO. The bonding effect of the doubly occupied σ MO is partly compensated by the destabilizing effect of the HOMO.

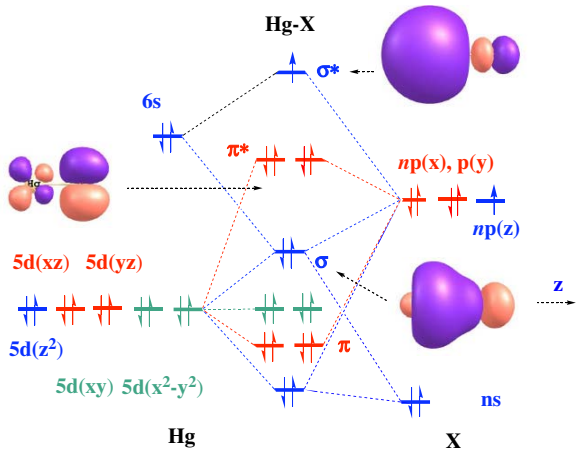

Fig. (2). Schematic presentation of the MO diagram of mercury halide HgX($^2\Sigma^+$). The 9 highest occupied MOs are shown. The σ-orbitals (blue), π-orbitals (red), and non-bonding orbitals (green) are indicated. Some computer drawings of the calculated orbitals for X = F are given.

Cremer and co-workers [79] determined the magnitude of the destabilization energy Δ caused by occupying the antibonding σ^* MO with the help of the thermodynamic cycle shown in Fig. (**3**). The IP of HgX when compared with the first IP of mercury provides a measure for the σ^*-destabilization Δ relative to the energy of the 6s(Hg) orbital. The destabilization energy Δ is exactly equal to the difference in the BDEs of neutral HgX and its cation HgX^+. The BDE values of the cations are up to 31 kcal/mol larger than those of their neutral counterparts, which is shown in Fig. (**4**) (NESC/CCSD(T) BDE values of HgX in blue, those of HgX^+ in red).

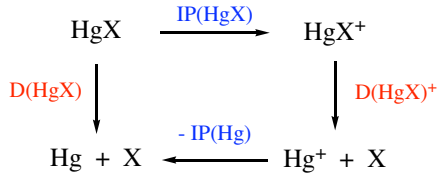

Destabilization of HOMO: IP(HgX) - IP(Hg)

= D(HgX) - D(HgX^+)

Fig. (3). Thermodynamic cycle to determine the destabilization energy Δ of the σ^*(HgX) MO of Fig. **2**. IP: Ionization potential, BDE: bond dissociation energy.

The destabilization Δ of the σ^* MO should be lowest for X being a strongly electronegative partner that prefers to undergo polar or ionic bonding whereas it should be largest for a bonding partner that prefers to bind covalently [79]. In the first case, the starting atomic orbitals (AOs) have strongly different energies, the ionic character of the bond is large, and the change in the energies of σ and σ^* MO relative to those of the AOs is moderate upon bonding. For example for X = F, the destabilization energy Δ is just 7.4 kcal/mol (see Fig. **4**). For X = I, the energies of the 6s(Hg) and the 5pσ(I) AOs are closer in energy, overlap between them is improved, and accordingly the splitting of the σ and σ^* MOs of HgI is larger thus leading to an increase in Δ to 36.3 kcal/mol, i.e. the BDE of HgI is just 10.9 kcal/mol due to a large Δ value, whereas the BDE value of HgI^+ is 47.2 kcal/mol because the σ^* MO is no longer occupied. This explains the observed inversion in the trends of the BDE values of HgX and HgX^+ when changing X from F to I. The HgI bond has the highest covalent character, which implies a large splitting between σ and σ^* MO and, consequently, a large destabilization energy Δ.

As shown in Fig. (**4**), the HgX bond strength increases for the monocations within a group and from right to left within a period up to group IVB. In a similar way, the destabilization Δ of the σ^*(HgX) MO increases (up to 83

NESC/CCSD(T):	Hg-X energy	HgX^+ energy	σ* destabilization energy

H	10.0										
50.9	60.9										
Li	2.9	**CH_3**	3.0	**NH_2**	4.2	**OH**	12.3	**O**	3.8	**F**	30.9
10.9	13.8	66.2	69.2	45.8	50.0	27.6	39.9	14.8	18.6	7.4	38.3
Na	2.3	**SiH_3**	6.3	**PH_2**	3.6	**SH**	9.7	**S**	5.7	**Cl**	21.4
3.9	6.2	78.3	84.6	60.2	63.8	40.6	50.3	34.5	40.2	20.6	42.0
K	0.8	**GeH_3**	5.4	**AsH_2**	4.5	**SeH**	7.5	**Se**	3.7	**Br**	14.4
4.2	5.0	79.1	84.5	62.2	66.7	44.0	51.5	37.9	41.6	25.1	39.5
Rb	0.7	**SnH_3**	3.0	**SbH_2**	1.9	**TeH**	5.9	**Te**	2.6	**I**	10.9
3.7	4.4	83.3	86.3	70.0	71.9	52.8	58.7	49.2	51.8	36.3	47.2

Fig. (4). NESC/CCSD(T) BDE values of 25 HgX molecules (in blue) and their corresponding cations HgX^+ (in red). The destabilization energy of the σ^* MO, calculated according to the thermodynamic cycle of Fig. (**3**), is also given (in black below X) [6].

kcal/mol, X = SnH_3) so that as a consequence the HgX bond strength decreases (just 3 kcal/mol for X = SnH_3). All HgX molecules, with the exception of the mercury halides, possess BDE values between 3 and 12 kcal/mol. For the corresponding cations the bond strength is much larger (up to 86 kcal/mol, Fig. **4**) thus reflecting the actual strength of 2-electron bonding.

It has to be noted that for HgX molecules with X being an alkali atom, dissociation into Hg + X^+ takes place, which has to be considered in the thermodynamic cycle of Fig. (**3**). The destabilization Δ in this case is that of the σ^* MO relative to the highest occupied ns(A) orbital (A = Li, Na, K, Rb). Since alkali metals are electron donors rather than electron acceptor, BDE values of both HgA and and HgA^+ are relatively small, small Δ values result, and bonding is reminiscent of a van der Waals complex rather than a covalently bonded molecule (Fig. **4**) [79]. In the case of true van der Waals complexes, the BDE would have to increase, e.g. within the series HgLi, HgNa, HgK, HgRb according to an increase of the polarizability with the volume of the alkali atom. However, just the opposite trend is observed (Fig. **3**). Clearly, a small BDE is not always indicative of the existence of a van der Waals complex. In the vase of the HgX molecules, relatively strong covalent bonding (for electronegative X groups changing to partially ionic bonding) is significantly reduced by occupying a σ^* MO.

As shown in Fig. (**2**), a set of π^* MOs, formed from the $5d\pi$(Hg) and $np\pi$(X) AOs is occupied in the $HgX(^2\Sigma^+)$ ground state. This leads to additional destabilization, which is commonly addressed as lone pair, lone pair repulsion. The stabilization caused by the occupation of the π-bonding MO is offset by the antibonding π MO and causes additional destabilization, the magnitude of which can be estimated by comparing the IP of the 5d(Hg) (IP3 in Table **1**) and that of the $np\pi$(X) orbital. The values are 34.5 eV for Hg and 34.9, 23.8, 21.8, and 19.1 eV for F, Cl, Br, and I, respectively [76]. According to this comparison, the π^*-destabilization (and thereby bond weakening because of lone pair repulsion) should be strongest for F and weakest for I.

In summary, the strongest scalar relativistic effect is the contraction of the 6s(Hg) AO. It has three major consequences for HgX bonding: i) The 6s AO energy decreases and directly affects the magnitude of the σ^*-destabilization energy Δ. ii) The decrease in the 6s AO energy makes charge transfer from Hg to X more difficult and thus reduces the polar character and the strength of the HgX bond. iii) The relativistic ns(Hg) AO contraction leads to a shielding of the Hg nucleus thus lowering its effective atomic charge for the 5d(Hg) electrons. The 5d orbitals expand and their orbital energies increase in value. This leads to a change in lone pair repulsion (π^* destabilization), which is reflected by the relativistic corrections of the BDE values (see Fig. **1**). They are always negative where their magnitude depends on the number of electron lone pairs of atom or group X: large relativistic corrections are determined for the halogen atoms and small ones for the alkali atoms. Within a group, the absolute value of the relativistic correction becomes smaller where from F to Cl (O to S; NH_2 to PH_2) a sudden drop of 5 to 6 kcal/mol can be observed. This drop reflects the relativistic 5d(Hg)-expansion and the subsequent adjustment of $5d\pi$(Hg) and $np\pi$(X) AO energies: lone pair repulsion becomes significant in the case of the second row atoms and leads to another weakening of the HgX bond.

3.3. Influence of Spin-Orbit Coupling on the Stability of Mercury Containing Molecules

Filatov and co-workers have developed a 2-component NESC method that provides spin-orbit coupling (SOC) corrected BDE values and other reaction energies [80]. Utilizing their 2-component NESC method in connection with the PBE0 functional, the energies of Tables **2** and **3** are obtained, which reveal the impact of SOC on energies of six different dissociation (atomization) energies (R1 - R6) for mercury halides of the type HgX_n (X = F, Cl, Br, I , At; n = 1, 2, 4).

If the reaction involves just closed-shell systems as in the case of R1, R2, and R5, the SOC corrections are in the range

Table 2. NESC/PBE0 energies (in kcal/mol) of HgX_n (X = H, F, Cl, Br, I, At) dissociation and atomization reactions. [a]

X	ΔE	ΔH^o_{298}	ΔG^o_{298}	X	ΔE	ΔH^o_{298}	ΔG^o_{298}
(R1): $HgX_4 \rightarrow HgX_2 + X_2$				(R2): $HgX_4 \rightarrow Hg + 2X_2$			
H	-39.5	-41.1	-48.9	H	-55.0	-57.0	-71.4
F	13.6	12.9	2.5	F	104.1	103.2	84.8
Cl	-33.9	-34.4	-44.2	Cl	17.0	16.1	-1.5
Br	-33.7	-34.3	-43.8	Br	10.8	9.9	-7.3
I	-29.7	-30.3	-39.3	I	10.5	9.5	-7.2
At	-31.5	-30.5	-42.4	At	-1.3	-2.2	-17.9
(R3): $HgX_4 \rightarrow Hg + 4X$				(R4): $HgX \rightarrow Hg + X$			
H	153.9	141.0	112.6	H	11.8	10.8	5.8
F	174.4	172.1	139.4	F	34.0	34.1	28.6
Cl	136.2	135.3	104.1	Cl	27.0	27.2	22.1
Br	115.2	114.6	84.1	Br	21.9	22.2	17.1
I	93.3	92.9	63.5	I	16.2	16.5	11.6
At	84.2	83.8	55.5	At	13.9	14.2	9.4
(R5): $HgX_2 \rightarrow Hg + X_2$				(R6): $HgX_2 \rightarrow Hg + 2X$			
H	-15.5	-15.9	-22.4	H	88.9	83.1	69.6
F	90.5	90.3	82.3	F	125.6	124.7	109.6
Cl	50.9	50.6	42.8	Cl	110.5	110.1	95.5
Br	44.5	44.2	36.5	Br	96.7	96.6	82.2
I	40.1	39.8	32.2	I	81.6	81.5	67.5
At	30.2	30.2	24.4	At	73.0	73.2	61.1

[a]Obtained with the PBE0 functional [81] and with a NESC-recontracted def2-QZVPP basis set for light atoms (H-Br) [82, 83] and a NESC-recontracted SARC basis for heavy atoms [82, 84, 85].

of 1 - 3 kcal/mol and lead to a slight reduction of the exothermicity (R1) or endothermicity (R2, R4) of the reaction. An exception is only found when HgAt is involved in the reaction: Then, the changes in the reaction energy of R1 and R2 are 15.6 and 14.1 kcal/mol. Since such a change is not observed for reaction R5, the calculated energies suggest that the SOC is important for the correct description of $HgAt_4$. In general one can say that significant SOC corrections result from a fractional occupation of p-, d-, and/or f-orbitals of a relativistic atom or molecule. The closed-shell molecule $HgAt_4$ is an exception from this rule.

For the reactions R3, R4, and R6, which involve the open-shell $X(^2P)$ atoms, the SOC corrections change from slightly positive too strongly negative values lowering the atomization energies of $HgAt_4$ (R3), $HgAt_2$ (R6), and HgAt (R4) by 40.1, 28.6, and 10.5 kcaL/mol, respectively, which suggest a 10 kcal/mol SOC correction per At atom. Hence, the SOC correction is always needed for high accuracy calculations.

The reaction energies of Table **3** reveal that only for X = F, the standard dissociation enthalpy at 298 K, ΔH^o_{298}, of HgX_4 is endothermic by 15 kcal/mol. Entropy effects lower this value to a dissociation free energy at 298 K, ΔG^o_{298}, of just 4 kcal/mol, i.e. at room temperature dissociation of HgF_4 is spontaneous. This is in line with the fact that so far HgF_4 could only be observed under the conditions of matrix isolation spectroscopy [78]. Other dissociation channels such as those of R2 and R3 (atomization) are strongly positive for HgF_4 (ΔE = 106.8 and 190.2 kcal/mol) whereas for X = H, Cl, Br, I, and At much smaller or even negative values are found. For example in the case of HgH_4, the formation of H_2 molecules becomes exothermic in view of the HH bond strength of 109 kcal/mol. This suggests that HgF_4 is thermodynamically stable because the F_2 molecule has a low stabilization energy according to a BDH value of 37.9 kcal/mol [44]. Apart from HgF_4 all other mercurytetrahalogenides are thermodynamically unstable. In the following, we will analyze Hg-X bonding by investigating the local stretching force constant and the HgX bond order.

Table 3. NESC/PBE0 energies (in kcal/mol) of HgX_n (X = H, F, Cl, Br, I, At) dissociation and atomization reactions including SOC corrections.[a]

X	ΔE	ΔH^{o}_{298}	ΔG^{o}_{298}	X	ΔE	ΔH^{o}_{298}	ΔG^{o}_{298}
(R1): $HgX_4 \rightarrow HgX_2 + X_2$				(R2): $HgX_4 \rightarrow Hg + 2X_2$			
H	-38.7	-40.3	-48.2	H	-52.6	-54.7	-69.0
F	15.7	15.0	4.6	F	106.8	106.0	87.6
Cl	-32.9	-33.4	-43.3	Cl	18.7	17.9	0.2
Br	-32.8	-33.4	-42.8	Br	12.4	11.5	-5.7
I	-26.7	-27.3	-36.4	I	13.9	12.9	-3.8
At	-15.9	-16.8	-26.8	At	12.8	11.9	-3.8
(R3): $HgX_4 \rightarrow Hg + 4X$				(R4): $HgX \rightarrow Hg + X$			
H	156.8	143.9	115.5	H	12.8	11.8	6.8
F	190.2	187.9	155.2	F	37.5	37.6	32.2
Cl	137.1	136.1	104.9	Cl	27.2	27.4	22.2
Br	104.3	103.8	73.3	Br	19.2	19.4	14.4
I	72.5	72.1	42.7	I	10.8	11.1	6.2
At	44.1	43.7	15.4	At	3.4	3.7	-1.1
(R5): $HgX_2 \rightarrow Hg + X_2$				(R6): $HgX_2 \rightarrow Hg + 2X$			
H	-13.9	-14.3	-20.8	H	90.8	84.9	71.4
F	91.2	91.0	83.0	F	132.8	132.0	116.8
Cl	51.6	51.3	43.5	Cl	110.8	110.4	95.8
Br	45.2	44.9	37.2	Br	91.2	91.0	76.6
I	40.6	40.3	32.6	I	69.9	69.8	55.9
At	28.7	28.7	22.9	At	44.4	44.6	32.5

[a]For details of the calculations, see Table **2**.

3.4. The Strength of the HgX Bond in Mercury Halides

In Table **4**, NESC/PBE0 frequencies of HgX, HgX_2, and HgX_4 are listed. These have been used to derive NESC/PBE0 local HgX stretching frequencies $\omega^a(HgX)$ and force constants $k^a(HgX)$ summarized in Table **5**. To derive a relative bond strength order (RBSO) n, we choose HgF_2 and HgF as suitable references and set the RBSO value of the former equal to 1 and that of the latter equal to 0.5 in view of the fact that the HOMO is a σ^* MO and singly occupied (see Fig. **2**). Actually, we should consider also the Δ destabilization value of 7.4 kcal/mol (Fig. **4**). However, for the purpose of obtaining just trends in the calculated bond strength, a simplified determination of RBSO values is justified. A power relationship between n and k^a is derived by setting $n = 0$ for $k^a = 0$ and using the reference values for HgF_2 and HgF. Utilizing this power relationship, the RBSO values of Table **5** are determined from the calculated NESC/PBE0 HgX stretching force constants.

According to the calculated RBSO values, bonding in HgX_2 molecules is strongest for a given X, however with the exception of X = F and X = H for which bonding turns out to be stronger in HgX_4. The bond strength in $HgX(^2\Sigma^+)$ is just 40 - 50% of that in HgX_2 ($^1\Sigma_g^+$). For HgX_4 it is 105, 107, 84, 77, 69 and 67% of the value in HgX_2. For all HgX_n molecules there is a steady decrease in the bond strength from X = F to X = At, where the latter element forms very weak bonds with Hg (BDE = 3.4 and $n = 0.163$ for $HgAt(^2\Sigma^+)$). Cremer and co-workers [79] have argued that the bond strength changes with the electronegativity of X and the amount of electron density transferred from the Hg atom to the X atom. To clarify this argument, in Fig. (**5**) the RBSO values n are given as a function of the NBO charge values of X , which reflect the charge transfer from Hg to X.

There are quadratic or exponential relationships between n and the NBO charge of X where only the HgX_n molecules with X = H do not follow these relationships because the bonding mechanism is different involving s- rather than $np\sigma$ -orbitals. There is an obvious dependence on the electronegativity of X and the charge transfer from Hg to X, which is largest for X = F and smallest for X = At in view of Allred-Rochow electronegativities of 4.10 (F), 2.83 (Cl), 2.74 (Br), 2.21 (I), and 1.90 (At) (H: 2.20 is comparable to the electronegativity of I) [86]. It is also obvious that HgF bonding is significantly stronger than for all other halogens as reflected by RBSO values being 40-50% larger than, e.g.,

HgCl bonds.There is also a difference between HgF bonding and HgX bonding as the strongest HgF bonds are found for HgF_4 whereas in all other halogenides HgX_2 has the strongest HgX bonds.

Table 4. Normal mode frequencies (in cm^{-1}) of HgX_n molecules (NESC/PBE0 calculations).[a]

X (state, symm.) [b]	ω^{μ}
HgX ($^2\Sigma^+$, $C_{\infty v}$)	
H	1349 (σ^+)
F	445 (σ^+)
Cl	273 (σ^+)
Br	178 (σ^+)
I	131 (σ^+)
At	105 (σ^+)
HgX_2 ($^1\Sigma_g^+$, $D_{\infty h}$)	
H	2077 (σ_g^+), 1964 (σ_u^+), 816 (π_u)
F	665 (σ_u^+), 590 (σ_g^+), 180 (π_u)
Cl	412 (σ_u^+), 359 (σ_g^+), 103 (π_u)
Br	291 (σ_u^+), 221 (σ_g^+), 69 (π_u)
I	232 (σ_u^+), 157 (σ_g^+), 52 (π_u)
At	199 (σ_u^+), 116 (σ_g^+), 43 (π_u)
HgX_4 ($^1A_{1g}$, D_{4h})	
H	2146 (b_{1g}), 2123 (a_{1g}), 2013 (e_u), 909 (b_{2u}), 857 (a_{2u}), 771 (e_u), 758 (b_{2g})
F	692 (e_u), 613 (a_{1g}), 607 (b_{1g}), 254 (e_u), 229 (a_{2u}), 228 (b_{2g}),176 (b_{2u})
Cl	382 (e_u), 337 (a_{1g}), 313 (b_{1g}), 147 (e_u), 146 (b_{2g}), 129 (a_{2u}), 72 (b_{2u})
Br	260 (e_u), 202 (a_{1g}), 183 (b_{1g}), 91 (e_u), 90 (a_{2u}), 83 (b_{2g}), 37 (b_{2u})
I	195 (e_u), 141 (a_{1g}), 121 (b_{1g}), 70 (a_{2u}), 67 (e_u), 55 (b_{2g}), 18 (b_{2u})
At	164 (e_u), 102 (a_{1g}), 88 (b_{1g}), 57 (a_{2u}), 45 (e_u), 18 (b_{2g}), 13 (b_{2u})

[a]For details of the calculations, see Table **2**.
[b]Electronic state and symmetry group are given in parentheses.

In Table **6**, the NESC/PBE0 NBO (natural bond orbital) electron configurations are shown. Three interesting observations can be made: i) For all HgX_n molecules the loss of 6s(Hg) electronic charge is largest for X = F: 1.43 e for n = 4; 1.16 e for n = 2, and 0.68 e for n = 1. For other X, these values are much smaller. ii) The general expectation that the formation of HgX_4 involves the 5d(Hg) orbitals and leads to a d^8 electron configuration cannot be confirmed. There is some d-involvement as reflected by the $5d^{9.25}$ configuration (compared to $5d^{9.75}$ and $5d^{9.92}$ electron configurations in the cases of HgF_2 and HgF), however the loss of charge from the 5d(Hg) orbitals is much smaller than expected. iii) There is a surprisingly high 6p(Hg) involvement with occupation numbers ranging from 0.32 (F) to 0.98 (I), 0.96 (At) and 1.04 (H). For HgX and HgX_2, these values are small (HgX: 0.1 - 0.2; HgX_2: 0.1 - 0.4).

The scalar relativistic MOs shown in Fig. (**6**) suggest a 5d-orbital participation in HgF bonding. In total, there are six MOs with strong or weak bonding character. Two low-lying MOs of b_{1g}- and a_{1g}-symmetry have strong bonding character where HgF bonding involves the $5d_{x^2-y^2}$ and $5d_{z^2}$ orbitals beside 6s and 6p contributions. Then, there are four weakly bonding.

MOs (b_{2g} at -18 eV, a_{1g} at -14 eV, and two e_g at -17.5 eV), which complement bonding in HgF_4. All higher lying occupied MOs are either nonbonding or weakly π-type antibonding (see Fig. **6**). Bonding in HgF_4 may be best characterized as electron deficient with a strong ionic character in view of a positive Hg charge of 1.82 e. Any bonding partner X, which cannot establish this ionic character because of a too low electronegativity forms HgX_2 rather than HgX_4. This is clearly reflected by the calculated RBSO values of HgX_4, which decrease from 1.072 (F) to 0.544 (Cl), 0.428 (Br), 0.310 (I), and 0.268 (At, Table **6**).

It remains to be clarified why there are (kinetically and thermodynamically) unstable HgX_4 molecules at all for the higher halogens since for each of these molecules an energy minimum is found in the NESC calculations. In view of the fact that the formation of a highly polar bond as in the case of X = F is not possible, electron density is promoted to the 6p orbital (see Table **6**) and some sp-hybridization takes place, which leads to weak electron deficient bonding.

CONCLUSIONS

In the last three years, the analytical derivatives formalism of the Dirac-exact NESC method has been introduced into the standard repertoire of quantum chemical tools so that the study of molecules with relativistic atoms has become routine. This opens up the possibility of a reliable description of heavy atom chemistry for nontrivial systems, which was not available for a long time. We have demonstrated some of the application potential of the Dirac-exact NESC method by focusing on the properties of mercury compounds. Experimental work on mercury reactions is limited by the toxic nature of many Hg-containing compounds. Nevertheless, a thorough study of mercury chemistry is highly desirable because of the role mercury plays as a toxic pollutant in the environment.

A thorough understanding of the reactivity of mercury compounds requires a detailed insight into mercury bonding. As demonstrated in this article, such an insight can be gained with the help of vibrational spectroscopy. A stretching vibration probes the strength of an HgX bond. By converting normal modes into local modes, reliable bond strength descriptors are obtained in form of the local HgX stretching

Table 5. Bond lengths R(HgX) in Å, local stretching force constants k [a](HgX) in mdyn/Å, local frequencies ω[a](HgX) in cm^{-1}, NBO charges q in e, and relative bond strength orders (RBSO) *n* of HgX_n molecules according to NESC/PBE0 calculations.[a]

X	R(Hg-X)	k [a] (Hg-X)	ω[a] (Hg-X)	q(Hg)	q(X)	n(Hg-X)
HgX ($C_{\infty v}$)						
H	1.747	1.075	1349	0.291	-0.291	0.264
F	2.039	2.025	445	0.654	-0.654	0.500
Cl	2.389	1.311	273	0.523	-0.523	0.323
Br	2.534	1.060	178	0.457	-0.457	0.261
I	2.736	0.794	131	0.352	-0.352	0.195
At	2.840	0.665	105	0.322	-0.322	0.163
HgX_2 ($D_{\infty h}$)						
H	1.639	2.406	2018	0.638	-0.319	0.595
F	1.910	4.030	628	1.300	-0.650	1.000
Cl	2.249	2.628	387	0.914	-0.457	0.650
Br	2.385	2.241	259	0.784	-0.392	0.554
I	2.571	1.811	199	0.566	-0.283	0.447
At	2.661	1.626	164	0.522	-0.261	0.401
HgX_4 (D_{4h})						
H	1.625	2.533	2070	0.216	-0.054	0.626
F	1.883	4.320	650	1.820	-0.455	1.072
Cl	2.295	2.200	354	0.796	-0.199	0.544
Br	2.455	1.735	228	0.552	-0.138	0.428
I	2.679	1.261	166	0.164	-0.041	0.310
At	2.779	1.092	134	0.160	-0.040	0.268

[a]For details of the calculations, see Table **2**.

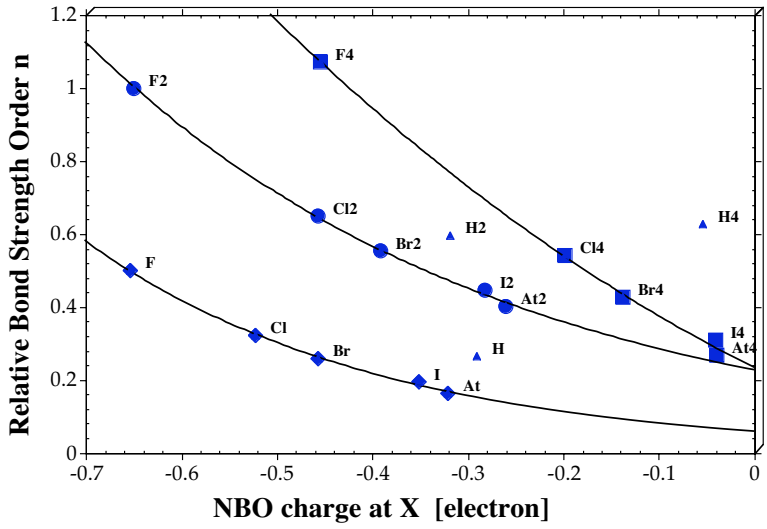

Fig. (5). Relative bond strength orders (RBSO) *n* plotted as a function of the relativistic NBO charge at halogen atom X. Abbreviations X, X2, and X4 (X = H, F, Cl, Br, I, At) denote molecules HgX, HgX_2, and HgX_4, respectively. (NESC/PBE0 calculations: For details, see Table **2**.)

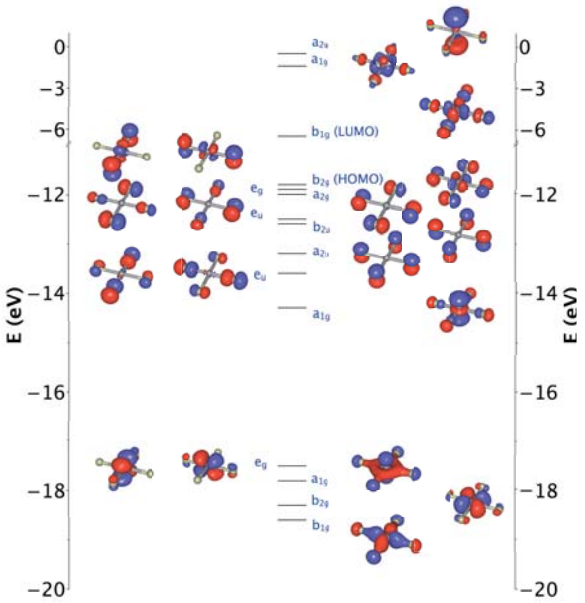

Fig. (6). MOs of HgF_4. NESC/PBE0 calculations.

Table 6. Valence electron configurations of Hg and X in HgX_n molecules. (NESC/PBE0 calculations). [a]

Molecule	Atom	Electron Configuration	Atom	Electron Config.
HgH_4	Hg	6s(1.03)5d(9.71)6p(1.04)	H	1s(1.05)
HgF_4	Hg	6s(0.57)5d(9.25)6p(0.32)	F	2s(1.95)2p(5.50)
$HgCl_4$	Hg	6s(0.81)5d(9.63)6p(0.73)	Cl	3s(1.92)3p(5.27)
$HgBr_4$	Hg	6s(0.88)5d(9.72)6p(0.81)	Br	4s(1.92)4p(5.21)
HgI_4	Hg	6s(1.00)5d(9.81)6p(0.98)	I	5s(1.90)5p(5.13)
$HgAt_4$	Hg	6s(1.01)5d(9.85)6p(0.96)	At	6s(1.93)6p(5.10)
HgH_2	Hg	6s(1.24)5d(9.89)6p(0.23)	H	1s(1.31)
HgF_2	Hg	6s(0.84)5d(9.75)6p(0.10)	F	2s(1.96)2p(5.68)
$HgCl_2$	Hg	6s(0.94)5d(9.87)6p(0.26)	Cl	3s(1.94)3p(5.50)
$HgBr_2$	Hg	6s(0.99)5d(9.90)6p(0.31)	Br	4s(1.94)4p(5.44)
HgI_2	Hg	6s(1.09)5d(9.93)6p(0.40)	I	5s(1.92)5p(5.35)
$HgAt_2$	Hg	6s(1.10)5d(9.94)6p(0.39)	At	6s(1.94)6p(5.32)
HgH	Hg	6s(1.59)5d(9.95)6p(0.16)	H	1s(1.29)
HgF	Hg	6s(1.32)5d(9.92)6p(0.10)	F	2s(1.98)2p(5.66)
HgCl	Hg	6s(1.38)5d(9.95)6p(0.13)	Cl	3s(1.97)3p(5.53)
HgBr	Hg	6s(1.44)5d(9.96)6p(0.13)	Br	4s(1.98)4p(5.47)
HgI	Hg	6s(1.53)5d(9.97)6p(0.14)	I	5s(1.97)5p(5.37)
HgAt	Hg	6s(1.57)5d(9.98)6p(0.12)	At	6s(1.98)6p(5.33)

[a]For details of the calculations, see Table **2**.

force constants and their associated RBSO values. This is demonstrated for HgX bonding in molecules of the type HgX_n (n = 1, 2, 4).

Relatively strong HgX bonding becomes possible when X is a strongly electronegative substituent such as F. Charge transfer from Hg to F leads to covalent bonding with strongly polar (ionic) character. Less electronegative bonding partners X form HgX molecules, which are characterized by small BDE values and which remind of van der Waals complexes. It has been shown that bonding in these cases is covalent, however weakened by a single electron occupation of a σ^*-orbital where the destabilization energy Δ can be estimated by a thermochemical cycle.

Mercurytetrahalides are only realized in the case of X = F as is documented by positive dissociation energies and relatively high RBSO values (n = 1.072) that are larger than for the reference bond in HgF_2 (n = 1.000). Bonding can be characterized as a mixture of covalent *electron-deficient* bonding and ionic bonding. A total of 1.82 e is transferred from Hg to the F atoms where most of the charge is taken from the 6s orbital and 0.75 e from the 5d orbitals of Hg. If the bonding partner of Hg has a lower electronegativity such as for X = Cl, Br, I, At bonding can only established by hybridization, i.e. a mixing of the 6s and 6p orbital where the latter obtains up to 1 e charge. This however requires a considerable amount of energy thus leading to relatively weak bonds as reflected by small RBSO values.

It is safe to say that HgF_4 is the only halogenide that has a chance of existing at low temperatures [78].

Future work has to show whether electronegative groups such as CF_3, NF_2, or OF present another possibility of realizing a Hg(IV) compound.

CONFLICT OF INTEREST

The authors confirm that this article content has no conflicts of interest.

ACKNOWLEDGEMENTS

Declared none.

REFERENCES

[1] Einstein, A. On the Electrodynamics of Moving Bodies. *Ann. Phys.,* **1905,** *17*, 891-893.

[2] Pyykkö, P. Relativistic Theory of Atoms and Molecules, A Bibliography; Lecture Notes in Chemistry, *Springer, Berlin*, **1986**, *41*, 1916-1985.

[3] Pyykkö, P. Relativistic effects in structural chemistry. *Chem. Rev.* **1988**, *88*, 563-594.

[4] Pyykkö, P. Relativistic Theory of Atoms and Molecules, A Bibliography 1986-1992, Lecture Notes in Chemistry, Vol. *60* Springer, Berlin, **1993**.

[5] Almlöf, J.; Gropen, O. In Reviews in Computational Chemistry, edited by K. B. Lipkowitz, D.; Boyd B. **1996**, *8*, 203-244.

[6] Schwerdtfeger, P.; Seth, M. *Encyclopedia of Computational Chemistry*, Vol *4*, edited by P. v. R. Schleyer, N. L. Allinger, T.; Clark, J.; Gasteiger, P. A.; Kollman, H. F.; Schaefer III; Schreiner J.W., *Chichester, UK*, **1998**, 2480.

[7] Dyall K.G.; Fægri, K. Introduction to Relativistic Quantum Chemistry. *Oxford University Press, Oxford,* **2007**.

[8] Grant I.P. Relativistic Quantum Theory of Atoms and Molecules, Theory and Computation. *Springer, New York,* **2007**.

[9] Reiher, M.; Wolf, A. Relativistic Quantum Chemistry, The Fundamental Theory of Molecular Science. *Wiley-VCH, Weinheim*, **2009**.

[10] Hess B.A.; Marian C.M. Computational Molecular Spectroscopy, edited by Jensen P.; Bunker, P.R. *Wiley, Sussex,* **2000**, 152-278.

[11] Liu, W. Ideas of relativistic quantum chemistry. *Mol. Phys.,* **2010**, *108*, 1679-1706.

[12] Saue, T. Relativistic Hamiltonians for Chemistry: A Primer. *ChemPhysChem*, **2011**, *12*, 3077-3094.

[13] Peng, D.; Reiher, M. Exact decoupling of the relativistic Fock operator. *Theor. Chem. Acc.,* **2012**, *131*,1081.

[14] Dirac, P.A.M. Quantum Mechanics of Many-Electron Systems. *Proc. Roy. Soc. (London)*, **1929,***123*, 714-733.

[15] Dirac, P.A.M. The Quantum Theory of the Electron. *Proc. Roy. Soc.,* **1928**, *A117*, 610-624.

[16] Dyall, K.G. Interfacing relativistic and nonrelativistic methods. I. Normalized elimination of the small component in the modified Dirac equation. *J. Chem. Phys.,* **1997**, *106*, 9618-9626.

[17] Dyall, K.G. An exact separation of the spin-free and spin-dependent terms of the Dirac-Coulomb-Breit Hamiltonian. *J. Chem. Phys.,* **1994**, *100*, 2118-2127.

[18] Kutzelnigg, W. Perturbation theory of relativistic corrections. *Z. Phys. D*, **1989**, *11*, 15-28.

[19] Kutzelnigg, W. Perturbation theory of relativistic corrections. *Z. Phys. D*, **1990**, *15*, 27-50.

[20] Zou, W.; Filatov, M.; Cremer, D. An improved algorithm for the normalized elimination of the small-component method. *Theor. Chem. Acc.,* **2011**, *130*, 633-644.

[21] Kutzelnigg, W.; Liu, W. Quasirelativistic theory equivalent to fully relativistic theory. *J. Chem. Phys.,* **2005**, *123*, 241102.

[22] Kutzelnigg, W.; Liu, W. Quasirelativistic theory I. Theory in terms of a quasi-relativistic operator. *Mol. Phys.,* **2006**, *104*, 2225-2240.

[23] Liu, W.; Kutzelnigg, W. Quasirelativistic theory. II. Theory at matrix level. *J. Chem. Phys.,* **2007**, *126*, 114107.

[24] Iliaš, M.; Jensen, H. J.; Roos, B. O.; Urban, M. Theoretical study of PbO and the PbO anion. *Chem. Phys. Lett.,* **2005**, *408*, 210-215.

[25] Filatov, M. *J. Chem. Phys.,* **2006**, *125*, 107101.

[26] Chang, C.; Pelissier, M.; Durand, P. Regular Two-Component Pauli-Like Effective Hamiltonians in Dirac Theory. *Phys. Scr.*, **1986**, *34*, 394-404.

[27] van Lenthe, E.; Baerends, E.J.; Snijders, J.G. Relativistic Regular Two-Component Hamiltonians. *J. Chem. Phys.,* **1993**, *99*, 4597-4610.

[28] van Lenthe, E.; Baerends, E.J. and Snijders, J.G. Relativistic total energy using regular approximations. *J. Chem. Phys.,* **1994**, *101*, 9783-9792.

[29] van Lenthe, E.; Ehlers, A.; Baerends, E.J. Geometry optimizations in the zero order regular approximation for relativistic effects. *J. Chem. Phys.,* **1999**, *110*, 8943-8953.

[30] Dyall, K.G.; van Lenthe, E. Relativistic regular approximations revisited: An infinite-order relativistic approximation. *J. Chem. Phys.*, **1999**, *111*, 1366-1372.

[31] Filatov, M.; Cremer, D. Representation of the exact relativistic electronic Hamiltonian within the regular approximation. *J. Chem. Phys.,* **2003**, *119*, 11526-11540.

[32] Filatov, M.; Cremer, D. Connection between the regular approximation and the normalized elimination of the small component in relativistic quantum theory. *J. Chem. Phys.,* **2005**, *122*, 064104.

[33] Zou, W.; Filatov, M.; Cremer, D. Development and Application of the Analytical Energy Gradient for the Normalized Elimination of the Small Component Method. *J. Chem. Phys.,* **2011**, *134*, 244117.

[34] Filatov, M.; Zou, W.; Cremer, D. Analytic calculation of isotropic hyperfine structure constant using the normalized elimination of the small component formalism. *J. Phys. Chem. A*, **2012,** *116*, 3481-3486.

[35] Filatov, M.; Zou, W.; Cremer, D. Analytic calculation of contact densities and Mössbauer isomer shifts using the normalized elimination of the small component formalism. *J. Chem. Theor. Comput.,* **2012**, *8*, 875-882.

[36] Filatov, M.; Zou, W.; Cremer, D. Relativistically corrected Electric Field Gradients calculated with the Normalized Elimination of the Small Component Formalism. *J. Chem. Phys.,* **2012**, *137*, 054113.

[37] Zou, W.; Filatov, M.; Cremer, D. Development, Implementation, and Application of an Analytic Second Derivative Formalism for the Normalized Elimination of the Small Component Method. *J. Chem. Theory Comput.,* **2012**, *8*, 2617-2629.

[38] Zou, W.; Filatov, M.; Cremer, D. Analytic calculation of second-order electric response properties with the normalized elimination of the small component (NESC) method. *J. Chem. Phys.,* **2012**, *137*, 084108.

[39] Filatov, M.; Zou, W.; Cremer, D. On the isotope anomaly of nuclear quadrupole coupling in molecules. *J. Chem. Phys.,* **2012**, *137*, 131102.

[40] Liu, W.; Peng, D. Exact two-component Hamiltonians revisited. *J. Chem. Phys.,* **2009**, *131*, 031104.

[41] Yamaguchi, Y.; Goddard, J.D.; Osamura, Y.; Schaefer, H.F.S. A New Dimension to Quantum Chemistry: Analytic Derivative Methods in *Ab Initio* Molecular Electronic Structure Theory. Oxford University Press, Oxford, **1994**.

[42] Pople, J.A.; Krishnan, R.; Schlegel, H.B.; Binkley, J.S. Derivative studies in Hartree-Fock and Møller-Plesset theories. *Int. J. Quantum. Chem. Quantum Chem. Symp.,* **1979**, *13*, 225-241.
[43] Chase, M.W. NIST-JANAF Themochemical Tables, Fourth Edition. *J. Phys. Chem. Ref. Data Monograph*, **1998**, *9*, 1-1951.
[44] Luo, Y. Comprehensive Handbook of Chemical Bond Energies, CRC Press, Boca Raton, **2007**.
[45] Pauling, L. The Nature of the Chemical Bond and the Structure of Molecules and Crystals, An Introduction to Modern Structural Chemistry. Cornell University Press, **1960**.
[46] Slater, J.C. Directed Valence in Polyatomic Molecules. *Phys. Rev.,* **1931**, *37*, 481-489.
[47] Mulliken, R.S. Overlap Integrals and Chemical Binding. *J. Am. Chem. Soc.,* **1950**, *72*, 4493-4503.
[48] Cremer, D.; Wu, A.; Larsson, A.; Kraka, E. *J. Mol. Model*. **2000**, *6*, 396.
[49] Kalescky, R.; Kraka, E.; Cremer, D. Identification of the Strongest Bonds in Chemistry. *J. Phys. Chem. A,* **2013**, 117, 8981-95.
[50] Kraka, E.; Larsson, J.A.; Cremer, D. Generalization of the Badger Rule Based on the Use of Adiabatic Vibrational Modes in Vibrational Modes in Computational IR Spectroscopy. In Grunenberg, Jörg, editors, *Computational Spectroscopy: Methods, Experiments and Applications*, Wiley, New York, **2010**, pages 105.
[51] Badger, R.M. *J. Chem. Phys.,* **1934**, *2*, 128.
[52] Taylor, W.J.; Pitzer, K.S. *J. Res. Nat. Bureau Stand.,* **1947**, *38*, 1.
[53] Decius, J. *J. Chem. Phys.,* **1963**, *38*, 241.
[54] Brandhorst K.; Grunenberg, J. *Chem. Soc. Rev.* **2008**, *37*, 1558.
[55] Vijay, M.M.; Manoharan, S. *J. Chem. Phys.,* **2009**, *131*, 174112.
[56] Grunenberg, J.; Goldberg, N. Synthesis and reaction chemistry of homonuclear metal-metal bonded group 12 (zinc, cadmium and mercury) and group 13 (gallium and indium) organometallic compounds ArMMAr (Ar = terphenyl ligands) and related species. *J. Am. Chem. Soc.,* **2000**, *122*, 6045.
[57] Brandhorst K; Grunenberg, J. *J. Chem. Phys.* **2010**, *132*, 184101.
[58] Espinosa A.; Streubel, R.; *Chem. - Europ. J.*, **2011**, *17*, 3166.
[59] McKean, D.C. Relativistic effects in structural chemistry *Chem. Soc. Rev.,* **1978**, 7, 399.
[60] Duncan, J.L.; Harvie, J.L.; McKean, D.C.; Cradock, C. *J. Mol. Struct*. **1986**, *145*, 225.
[61] Murphy, W.F.; Zerbetto, F.; Duncan, J.L.; McKean, D.C. Experimental and ab initio infrared intensities in dimethylether: Atomic polar tensors and atomic charges. *J. Phys. Chem.,* **1993**, *97*, 581-586.
[62] Henry, B.R. *Acc. Chem. Res.,* **1987***, 20*, 429.
[63] Konkoli, Z.; Cremer, D. A new way of analyzing vibrational spectra. I. Derivation of adiabatic internal modes. *Int. J. Quantum. Chem.,* **1998**, *67*, 1-9.
[64] Konkoli, Z.; Cremer, D. A new way of analyzing vibrational spectra. III. Characterization of normal vibrational modes in terms of internal vibrational modes. *Int. J. Quantum. Chem.,* **1998**, *67*, 29-40.
[65] Konkoli, Z.; Larsson, J.A.; Cremer, D. *Int. J. Quant. Chem.,* **1998**, *67*, 11.
[66] Konkoli, Z; Larsson, J.A.; Cremer, D. *Int. J. Quant. Chem.,* **1998**, *67*, 41.
[67] Cremer, D.; Larsson, J.A.; Kraka, E. New Developments in the Analysis of Vibrational Spectra: On the Use of Adiabatic Internal Vibrational Modes. In Parkanyi, C., editors, *Theoretical and Computational Chemistry, Volume 5, Theoretical Organic Chemistry*. Elsevier, Amsterdam, **1998**, 259.
[68] Zou, W.; Kalescky, R.; Kraka, E.; Cremer, D. Relating normal vibrational modes to local vibrational modes with the help of an adiabatic connection scheme. *J. Chem. Phys.*, **2012**, *137*, 084114.
[69] Zou, W; Kalescky, R.; Kraka, E.; Cremer, D. Relating normal vibrational modes to local vibrational modes benzene and naphthalene. *J. Mol. Model,* **2012**, *19*, 1-13.
[70] Kraka, E.; Cremer, D. Characterization of CF bonds with multiple-bond character: bond lengths, stretching force constants, and bond dissociation energies. *ChemPhysChem.*, **2009**, *10*, 686-698.
[71] Freindorf, M.; Kraka, E.; Cremer, D. *Int. J. Quantum Chem*. **2012**, *112*, 3174.
[72] Kalescky, R; Zou, W.; Kraka, E.; Cremer, D. Local vibrational modes of the water dimer - Comparison of theory and experiment. *Chem. Phys. Lett.,* **2012**, *554*, 243-247.
[73] Kalescky, R.; Kraka, E.; Cremer, D. Local vibrational modes of the formic acid dimer - the strength of the double hydrogen bond. *Mol. Phys.* **2013**, *111*, 1497-1510.
[74] Wilson, E.B.; Decius, J.C.; Cross, P.C. *Molecular Vibrations. The Theory of Infrared and Raman Vibrational Spectra*. McGraw-Hill, New York, **1955**.
[75] Cremer, D.; Kraka, E. From molecular vibrations to bonding, chemical reactions, and reaction mechanism. *Curr. Org. Chem.* **2010**, *14*, 1524-1560.
[76] Haynes W.M. Handbook of Chemistry and Physics. 92 edition, CRC PRESS, **2011**.
[77] Jensen, W.B. Is Mercury Now a Transition Element? *J. Chem. Edu.,* **2008**, *85*, 1182-1183.
[78] Wang, X.; Andrews, L.; Riedel, R.; Kaupp, M. Mercury is a Transition Metal: The First Experimental Evidence for HgF_4. *Angew. Chem. Int. Ed. Engl,*. **2007**, *46,* 8371-8375.
[79] Cremer, D.; Kraka, E.; Filatov, M. *ChemPhysChem,* **2008**, *9*, 2510.
[80] Filatov, M.; Zou, W.; Cremer, D. Spin-orbit coupling calculations with the two-component Normalized Elimination of the Small Component method. *J. Chem. Phys.,* **2013**, *139*, 014106.
[81] Perdew, J.P.; Burke, K.; Ernzerhof, M. Generalized Gradient Approximation Made Simple. *Phys. Rev. Lett.,* **1996**, *77*, 3865-3868.
[82] EMSL Basis Set Exchange, https://bse.pnl.gov/bse/portal.
[83] Weigend, F.; Ahlrichs, R. Balanced basis sets of split valence, triple zeta valence and quadruple zeta valence quality for H to Rn: Design and assessment of accuracy. *Phys. Chem. Chem. Phys.,* **2005**, *7*, 3297-3305.
[84] Pantazis, D.A.; Chen, X.-Y.; Landis C.R.; Neese, F. All-Electron Scalar Relativistic Basis Sets for Third-Row Transition Metal Atoms. *J. Chem. Theory Comput.,* **2008**, *4*, 908-919.
[85] Pantazis D.A.; Neese, F. All-electron scalar relativistic basis sets for the 6p elements. *Theor. Chem. Acc.,* **2012**, *131*, 1292.
[86] Porterfield, W.W. *Inorganic Chemistry, A Unified Approach*. Academic Press, San Diego, **1993**.

Received: November 03, 2013 **Revised: December 03, 2013** **Accepted: December 03, 2013**